This Page Is Inserted by IFW Operations
and is not a part of the Official Record

BEST AVAILABLE IMAGES

Defective images within this document are accurate representations of the original documents submitted by the applicant.

Defects in the images may include (but are not limited to):

- BLACK BORDERS
- TEXT CUT OFF AT TOP, BOTTOM OR SIDES
- FADED TEXT
- ILLEGIBLE TEXT
- SKEWED/SLANTED IMAGES
- COLORED PHOTOS
- BLACK OR VERY BLACK AND WHITE DARK PHOTOS
- GRAY SCALE DOCUMENTS

IMAGES ARE BEST AVAILABLE COPY.

As rescanning documents *will not* correct images, please do not report the images to the Image Problem Mailbox.

THIS PAGE BLANK (USPTO)

Methodology for Accurate and Rapid Simulation of Large Arbitrary 2D Layouts of Advanced Photomasks

Konstantinos Adam, Andrew R. Neureuther
EECS Department, University of California at Berkeley
Berkeley, CA 94720
email: kadam@eecs.berkeley.edu, neureuth@eecs.berkeley.edu

ABSTRACT

The edge domain decomposition method (edge-DDM) is developed as a very powerful extension of the domain decomposition methods presented in [1] for the rapid and accurate simulation of light scattering from advanced photomasks. The range of validity of the method is systematically evaluated and it is found to be accurate for wavelength-sized mask features with large vertical topography. The error associated primarily with neglecting corner effects is seen to concentrate at the extremities of the spectrum of propagating plane waves and is therefore filtered-out by the NA and the larger than one reduction factors in typical projection printing systems. A possible algorithmic implementation of the method, that involves rigorous pre-calculation of the edge-diffraction of all types of edges present in the layout, is presented for the simulation of large and arbitrary 2D layouts of alt. PSMs. A speed-up factor of 172,800 (1sec *vs.* 2days) is shown in the simulation of simple 3μm by 3μm (4X) 2D layouts (isolated hole and isolated island) with accuracy better than 99% compared to the rigorous 3D simulation of the mask diffraction. An example of the edge-DDM applied on a large 12μm by 16μm 2D layout of a 0°/90°/270° alt. PSM, where the near fields are estimated in less than 1min, is also presented. Spectral matching of the edge-diffraction with more compact piecewise constant models is shown to lead to additional speed-ups of the edge-DDM.

Keywords: domain decomposition method, edge-diffraction, phase-shift mask modeling, diffraction order

1. INTRODUCTION

Researchers have in the past investigated the decomposition of mask layouts into individual openings, and even into edges, for ideal thin masks under coherent illumination [6], but such techniques have never been applied to the rigorous solution for the scattered field. Domain decomposition techniques, where a large electromagnetic problem is broken up in smaller pieces and the final solution is arrived at by synthesizing (field-stitching) the elemental solutions, have been recently proposed for the study of one-dimensional binary (phase only) diffractive optical elements [5], [8]. Another research group working on the same problem demonstrated how to create and use a perturbation model for binary edge-transitions based on the product of the ideal, sharp transition and the continuous field variations in the vicinity of the edge [4]. Independently, a similar technique to field-stitching has been invented for the simulation of two-dimensional layouts of advanced photomasks (alternating PSM, masks with OPC) that properly models interactions from neighboring apertures and furthermore takes advantage of the spectral properties of the diffracted fields to come up with a compact model for the edge-transitions [1].

In this paper, a domain decomposition method based on edges is described, where the pre-calculated electromagnetic field from the diffraction of isolated edges is recycled in the synthesis of the near diffracted field from arbitrary two-dimensional diffracting geometries. Although at first glance it might be tempting to discard edge-decomposition techniques as inaccurate for masks with large vertical topography and features with small lateral dimensions, it will be shown that for a large set of practical situations they are very accurate. A key difference in this method from the one in [4] is that the sum of the complex

21st Annual BACUS Symposium on Photomask Technology
October 3, 2001
DTIC 10-3-01

fields is taken instead of the product. The reason for that lies in the linearity of the Kirchhoff-Fresnel diffraction integral [2] and it is exactly because of this linearity that the decomposition method is possible. The simulation program TEMPEST is used for all near field diffraction calculations [10], [7]. The simulation program SPLAT is employed for the imaging (far field) simulations [9]. By convention the thin mask model implied in SPLAT will be hereafter referred to as the *Kirchhoff-mask model*, or *k-mask*. Also, a *rigorous-mask model*, or *r-mask* will henceforth imply that a rigorously calculated near field by TEMPEST is fed into SPLAT for the subsequent modeling of the propagation into the projection system and the image formation.

The article is organized as follows: First, the new method for the mask domain decomposition is introduced and applied in simple 1D layouts. The limits of this method are systematically examined and presented next. Then, the method is expanded in 2D layouts and its algorithmic implementation for arbitrary layouts is considered. Simple 2D layouts that establish the validity and accuracy of the approach and large, arbitrary layouts that demonstrate its versatility are covered next. Finally, a very important direction for further enhancing the efficiency of the method that is based on spectral matching is discussed.

2. THE EDGE-DDM APPLIED IN 1D LAYOUTS

A natural extension of the domain decomposition method developed in [1] that is also based on the linearity of the Kirchhoff-Fresnel diffraction integral is shown in Figure 1. The 1D mask layout is first decomposed into single opening masks and subsequently each opening is decomposed into two edges and a uniform illumination field as in Figure 1. Such a decomposition can be proven to be exact for infinitely thin and perfectly conducting screens through the use of the electromagnetic form of Babinet's principle [3], but it should break down if applied to photomasks with "thick" vertical structures (compared to λ) and not perfectly absorbing screen materials. Also, due to the reduced ability of light to penetrate through very small (compared to λ) openings it is expected to break down for small mask features. This decomposition method will be hereafter

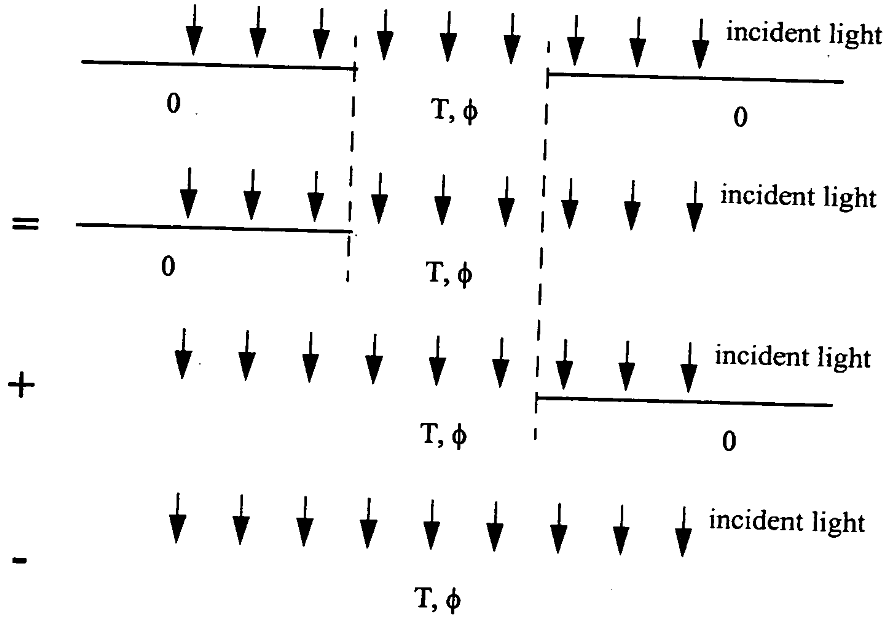

Figure 1. Decomposition of an opening into two edges

An opening with transmission T and phase ϕ in an infinitely thin, opaque screen can be decomposed by way of the linearity of the Kirchhoff-Fresnel diffraction integral into two edges. The uniform plane wave illumination is subtracted to restore the light level everywhere.

referred to as the *edge domain decomposition method* or *edge-DDM*. The application of the edge-DDM to a single isolated space and an isolated line are shown next, followed by a systematic evaluation of the limits of applicability of the method.

2.1. Decomposition of a space into two edges

Consider the isolated mask space (opening) shown in Figure 2(a). The amplitude of the complex E_y-field under E_y (TE) illumination is shown in (c) and the scattered field across the observation plane is shown in (e). According to Figure 1, the field across the observation plane can be alternatively obtained by using the scattered field from an edge that has the same vertical profile as the space, as shown in Figure 2(b) and (d). The resulting field from this edge-DDM is overlaid on the plot of Figure 2(e) along with the field from the edge scattering. The normalized mean square error[1] (NMSE) between the r-mask and the edge-DDM is 0.19%. In Figure 2(f) the spectra of the r-mask and edge-DDM are compared and it is seen that they differ by 0.13% in a NMSE sense if the whole spectrum of propagating waves is considered and by merely 0.007% within the collection

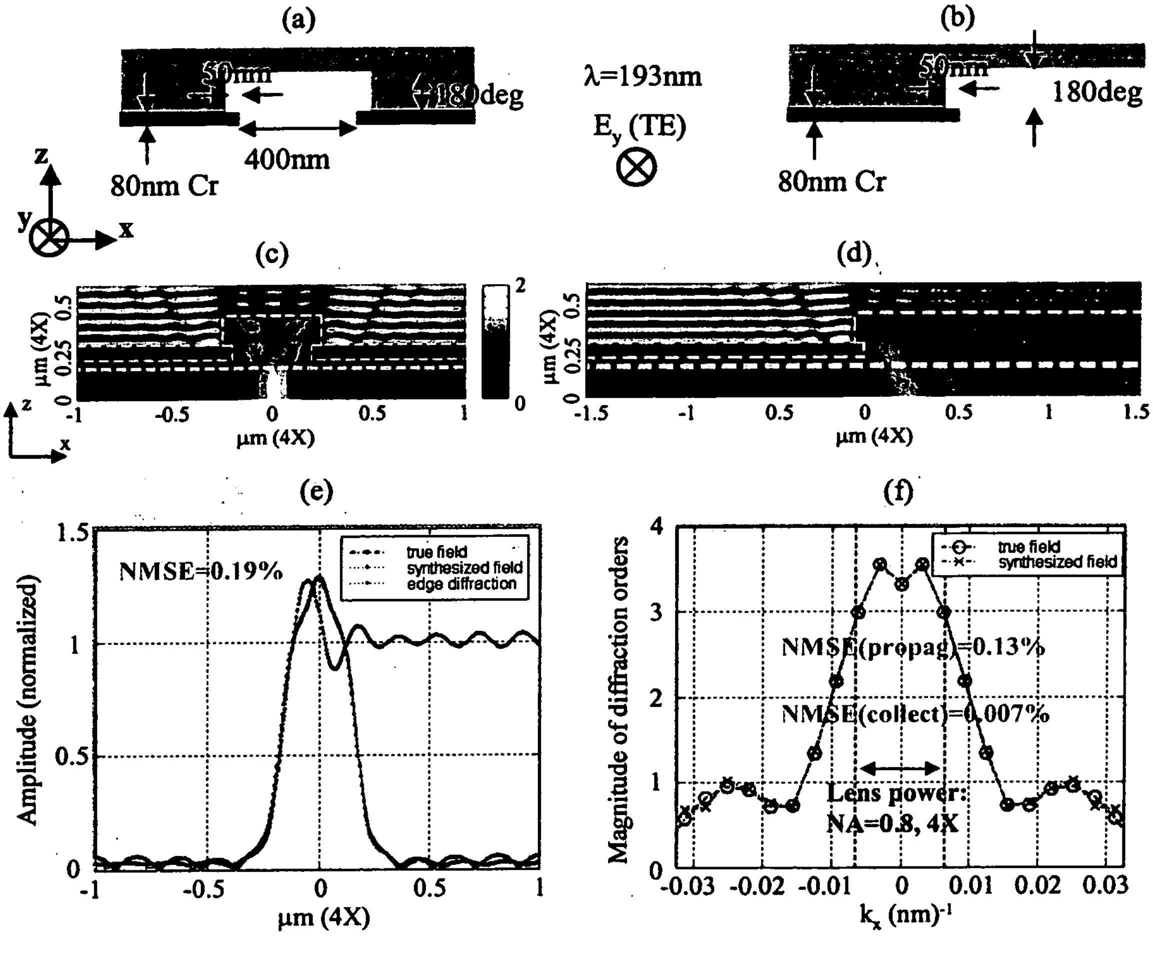

Figure 2. Edge-DDM applied on an isolated space

Geometry of mask with isolated space (a) and edge (b). Note that the vertical profile of the edge is the same as that of the isolated space. Amplitude of complex field from rigorous TEMPEST simulation for space (c) and edge (d). The true scattered field (r-mask) across the observation plane in (c) is compared with the edge-DDM (synthesized field) in (e) and their spectra are compared in (f). The normalized mean square errors (NMSE) are indicated on the plots.

---

[1] The normalized mean square error is defined by: $\mathrm{NMSE} = \int |E_r - E_s|^2 dS / \int |E_r|^2 dS$, where E_r is the "true" field resulting from a rigorous simulation of the complete mask geometry and E_s is the synthesized field *via* the edge-DDM.

ability of a projection system with NA=0.8 and R=4. Since only the portion of the spectrum that is collected by the projection system contributes to the image formation, the exceptional accuracy of the edge-DDM in this regime is more than adequate for accurate image simulations.

2.2. Decomposition of a line into two edges

Similar steps can be followed for the isolated line shown in Figure 3(a) illuminated with E_x (TM) polarized light. Note that it is not typical to have a line as shown here, where in both sides the glass has been etched. Normally only one side of the line is phase-shifted, but this example simply aims to introduce the principle of the edge-DDM. A line with one side phase-shifted and the other left intact can still be decomposed *via* the edge-DDM using the diffraction fields from the two different edges. The amplitude of the complex E_x field everywhere in the domain of Figure 3(a) is shown in (c) and for the edge of Figure 3(b) in (d) respectively. The true (r-mask) scattered field is compared with the synthesized field with edge-DDM in (e) and the spectra are compared in (f). The error (NMSE) is seen to be very small in both the near field and spectra plots and specifically the error of the through-the-lens (TTL) spectrum is just 1.5E-5.

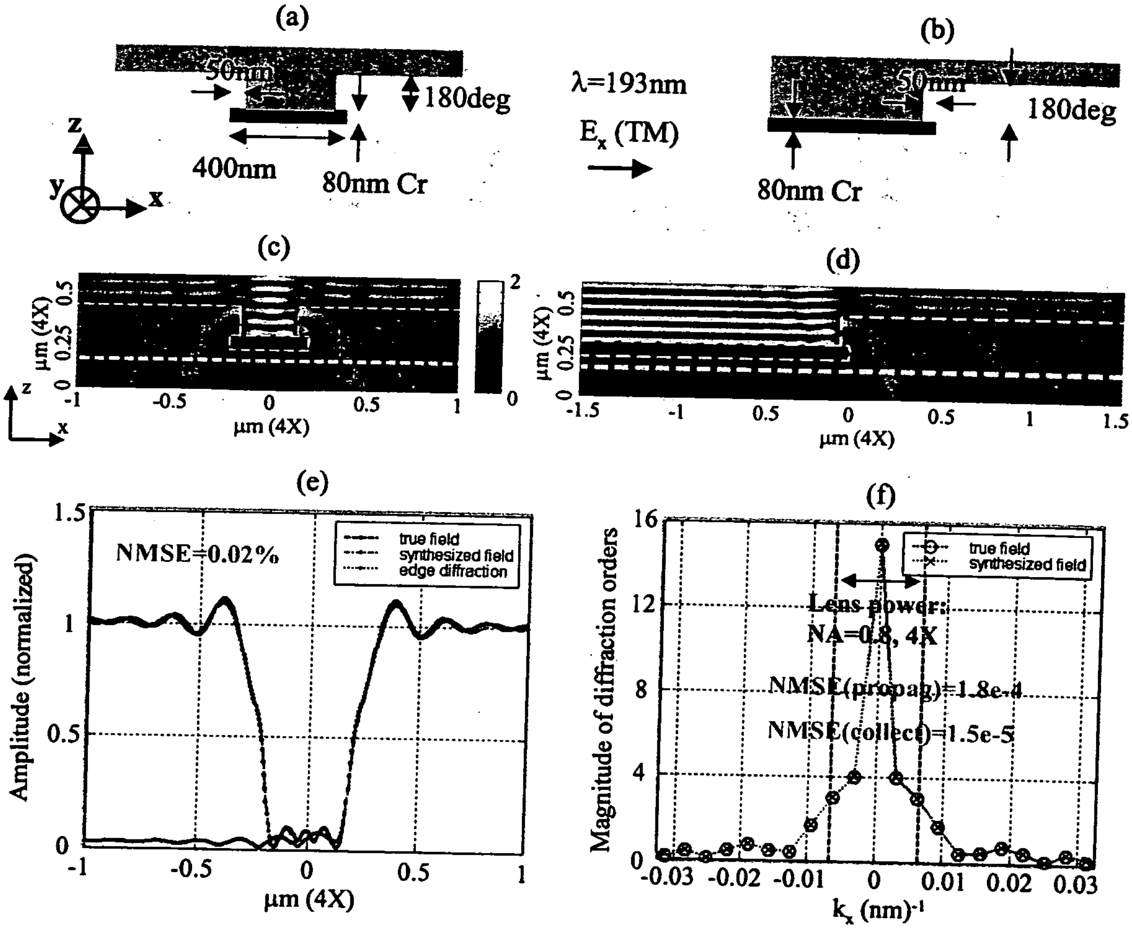

Figure 3. Edge-DDM applied on an isolated line

Geometry of mask with isolated line (a) and edge (b). Note that the vertical profile of the edge is the same as that of the isolated line. Amplitude of complex field from rigorous TEMPEST simulation for line (c) and edge (d). The true scattered field (r-mask) across the observation plane in (c) is compared with the edge-DDM (synthesized field) in (e) and their spectra are compared in (f). The normalized mean square errors (NMSE) are indicated on the plots.

2.3. Limits of the edge-DDM

In the examples of Figure 2 and Figure 3 the edge-DDM is seen to be very accurate compared with the simulation of the exact mask structure. Although the vertical mask topography ($180^{\circ} \approx 170\text{nm} \approx 1\lambda$) is comparable to the wavelength, the fact that the lateral dimensions of the space and the line are relatively large compared with the wavelength ($CD = 400\text{nm} > 2 \times 193\text{nm} = 2 \times \lambda$) renders the edge-DDM accurate. One expects that as the lateral sizes become smaller and the vertical mask topography even larger the edge-DDM will eventually break down. The limits of the edge-DDM were investigated through exhaustive simulation of isolated spaces and lines on the mask with various etched depths and amounts of undercut. The sidewall angles were always kept vertical and no rounding at the bottom of the etched wells was included. The mask CD was varied in the set {2µm, 1µm, 0.6µm, 0.4µm, 0.2µm(~1λ), 0.1µm}, the etched depth in {0°, 90°, 180°, 270°, 360°} and the amount of underetch in {0nm, 25nm, 50nm, 75nm, 100nm}. All 2 (space/line) by 2 (TE/TM illumination) by 6 (CD sizes) by 5 (etched depths) by 5 (underetch) = 600 cases were run and the rigorous (r-mask) scattered field was automatically compared with that obtained from edge-DDM. The results are spectacular! The edge-DDM can readily achieve better than 1% accuracy (in a NMSE sense) in the near field for CD=400nm (4X) or larger regardless of depth, underetch and polarization. The accuracy in the TTL-spectrum is sufficient in those cases even for inspection (R=1) simulations. For lines, the edge-DDM maintains excellent accuracy in the TTL-spectrum with R=4 down to a mask CD=100nm (~0.5λ) with 90° of etched depth and 0nm of undercut, or mask CD=200nm (~1λ) with 270° of etched depth and 25nm of undercut. For spaces, the accuracy of the method is acceptable at least down to mask CD=200nm (~1λ) with 270° of etched depth and 50nm of underetch.

Current state-of-the-art photomasks and processes utilize sub-resolution assist features that are never less than one wavelength in size on the mask. This clearly implies that the edge-DDM has the potential to accurately simulate the most advanced photomask technologies (OPC, alt. PSM, OPC on alt. PSM). As with the DDM of [1], the true power of the method lies on its application in 2D mask layouts. However, one key difference with the DDM of [1] is the following: Only one rigorous 2D simulation of an edge suffices for the scattered field reconstruction of *any arbitrary size on the mask!* The DDM of [1] requires a separate simulation of every different mask size. Next, the application of the edge-DDM in 2D layouts is developed.

3. THE EDGE-DDM APPLIED IN 2D LAYOUTS

The application of the edge-DDM in 2D layouts is straightforward. A mask layout comprises of a large number of edges positioned at different locations and having different orientations. No matter how complicated the mask technology is, there is usually only a small number of different types of edges present in the layout. For example, a single exposure 0°/90°/270° alt. PSM has five types of edges: i) Cr-layer/0° edge, ii) Cr-layer/90° edge, iii) Cr-layer/270° edge, iv) 0°/90° edge and 0°/270° edge. Depending on the orientation of each edge in the layout it "sees" and responds to the incident field differently. If the illuminating field is a TE (E_y) normally incident plane wave and the edge is oriented along the y-axis it "sees" TE illumination, but if it is oriented along the x-axis it "sees" TM illumination. This is illustrated in Figure 4. The response of each edge to its respective illumination is taken into account rigorously from a pre-stored 2D edge diffraction simulation. However, corner effects are effectively ignored, since the finite extent of each edge is not rigorously taken into account. Instead, the scattered field at the end points of every edge is abruptly terminated (truncated) in a perfect square-wave fashion to the field value of the k-mask model. Corner effects in typical imaging situations are mapped at the extremities of the spectra and do not contribute to the image formation. Due to this observation, which will be shortly proven valid in examples to follow, the edge-

DDM applied in 2D layouts is very successful in accurately capturing the true electromagnetic behavior of edges in a very rapid manner, while the insignificant corner effects are safely ignored.

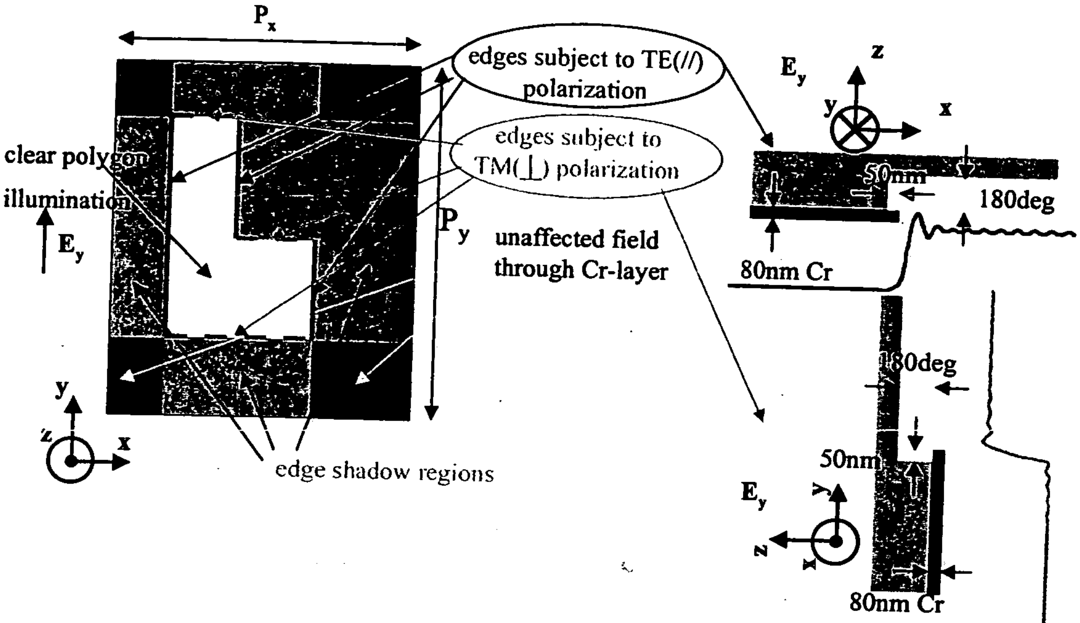
P$_x$
edges subject to TE(//) polarization
edges subject to TM(⊥) polarization
clear polygon illumination
E$_y$
P$_y$
unaffected field through Cr-layer
y
z
x
edge shadow regions
E$_y$
z
y
x
50nm
180deg
80nm Cr
180deg
50nm
E$_y$
80nm Cr

Figure 4. Edge-DDM applied on an arbitrary Manhattan-type polygon

Depending on the orientation of each edge in the layout it "sees" and responds to the incident field differently. Here the illuminating field is a TE (E_y) normally incident plane wave and the edges that are oriented along the y-axis "see" TE illumination (parallel to the edge), whereas the edges that are oriented along the x-axis "see" TM illumination (perpendicular to the edge). A separate 2D edge simulation is required to capture the different response of the edge to different field polarizations.

Slightly different embodiments of the edge-DDM applied in 2D layouts can be devised. One that is very powerful and general in its application is described next. Then, scattering results from various edge profiles that would be encountered in alt. PSMs are presented for completeness. Next, application of the edge-DDM in simple 2D mask layouts is presented and the results of the method are compared with fully rigorous r-mask models in order to establish the validity of this approach. Finally, a large portion of a real layout from a single exposure 0°/90°/270° alt. PSM that is too big for 3D rigorous simulation is simulated *via* the edge-DDM and the aerial image is compared with the simple k-mask model.

3.1. Algorithmic implementation of the edge-DDM

First, every distinct edge that is present on the layout is pre-simulated with all possible illumination directions (field polarizations) that are required, based on the orientations of the edge encountered within the layout. For simplicity only Manhattan-type layouts are considered, where the edges are oriented along either the x- or the y-axis and require electromagnetic simulation under both parallel and perpendicular to the edge polarizations. The extension to non-Manhattan layouts although much more computationally laborious is straightforward. Subsequently, each distinct mask layer is broken up into a set of mutually disjoint (non-overlapping) rectangles. For example, a plain binary mask consists of two layers, namely the absorption layer (typically Cr-based) and the clear (uncovered) layer, whereas a more advanced 0°/90°/270° three-phase alt. PSM consists of four layers, namely the absorption layer and the 0° clear, 90° clear and 270° clear layers. Next, looping through all rectangles of each layer, the type of each one of the four edges of the rectangle is determined based on what its neighboring layer is. Trivial edges (when the neighboring rectangle is of the same type) are discarded. It is also possible that only part of a single edge from a rectangle is neighboring with one layer and the rest is neighboring with a different layer (or different layers). In that case the edge is broken up in multiple edges, in a way that tracks the neighboring layer. What is left at the end of this process is a set of all non-trivial edges that are present in the layout (location, size and orientation) and their type, *i.e.* which are the two mask layers on each side of the edge. Given the mask layout, the k-mask (Kirchhoff-mask) model is readily available. Finally, the respective (complex) difference of the true edge scattering from the ideal and sharp k-mask model is added to all non-trivial edges accordingly. This revised mask model that results from the edge-DDM includes accurate information about the electromagnetic scattering from the edges and it can be thought of as a *quasi-rigorous mask model* (qr-mask) in the sense that only 2D rigorous mask simulations are used to approximate a 3D electromagnetic problem.

The above algorithm was implemented in the MATLAB environment. The part that deals with the polygon and edge extraction can probably be judged as rudimentary and most likely cannot compete in speed with more sophisticated implementations in production caliber CAD software, but it suffices for the purposes of this work, that is, to demonstrate the proof of concept of the edge-DDM and the feasibility of including very accurate edge scattering information in rapid aerial image simulations.

3.2. Dependence of edge scattering on profile and polarization

Examining the departure of the scattered field from an edge from its ideal, sharp edge transition and how it depends on the profile of the edge and the incident field polarization can provide great intuition of the physical mechanisms involved.

Figure 5 shows the amplitude of the (near) scattered field from an edge with various profiles. The ideal, sharp edge transition is also shown on every graph for comparison. In Figure 5(a) and (b) the edge scattering for different etched depths (0°, 180° and 360°) and vertical sidewalls with no undercut is shown for TE (E_y) and TM (E_x) illumination respectively. The effect of undercut is depicted in Figure 5(c) and (d), where the edge scattering for different amounts of undercut (0nm, 25nm, 50nm and 75nm) and vertical sidewalls with 180° etched depth is shown for TE and TM illumination respectively. It is interesting to note that increasing the etched depth is "making the edge response slower", meaning that the near scattered field from the edge requires more distance to reach its "on" value from its "off" value, although this effect is more pronounced for the first increment from 0° to 180° rather than from 180° to 360°. Similarly, increasing the amount of undercut appears to "make the edge response faster" and furthermore this behavior appears to be linear, since for every increment of the undercut the edge transition gains a constant distance in its "off-on" behavior.

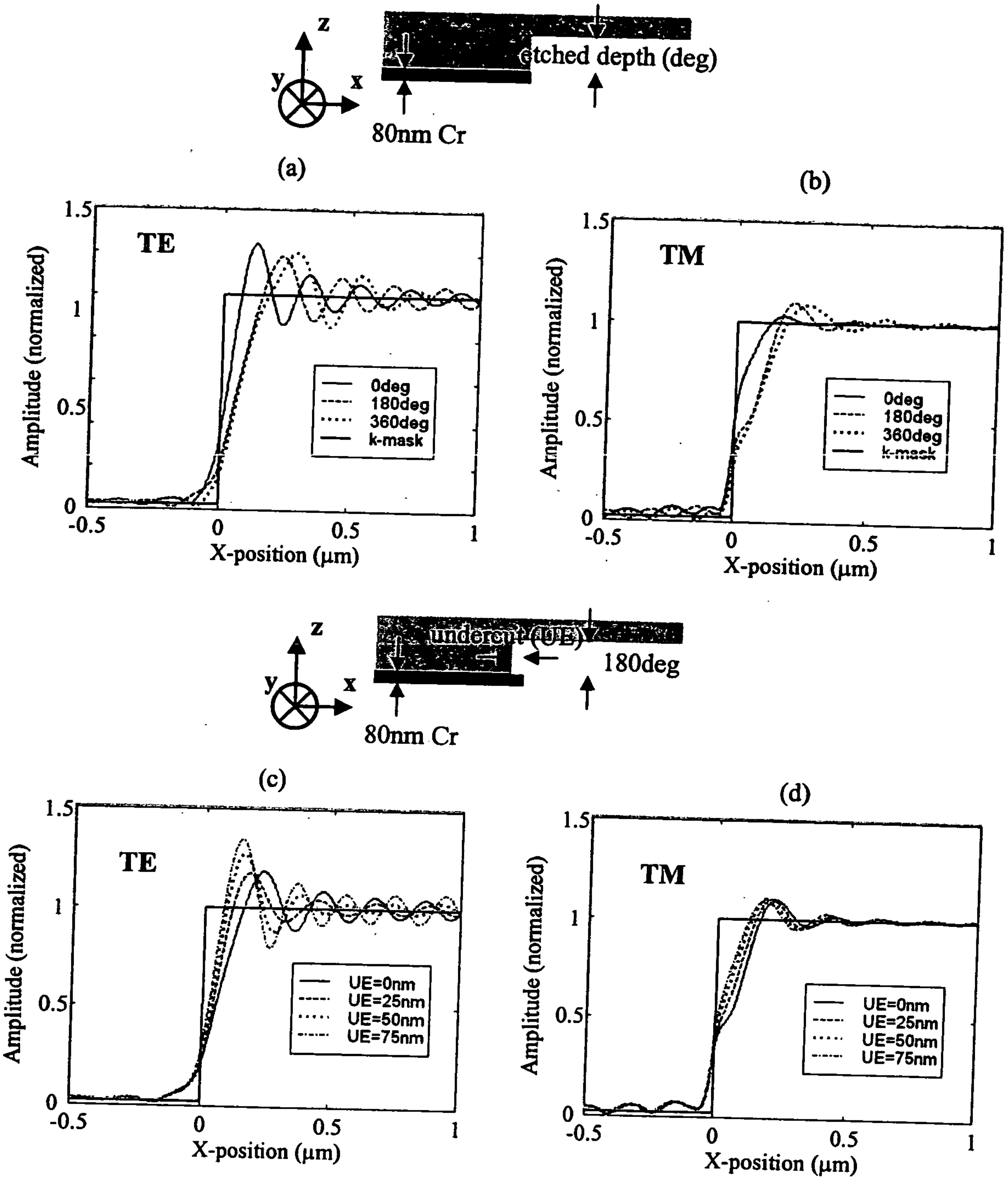

Figure 5. Dependence of edge scattering on profile and polarization

Normalized amplitude of the near field across the observation plane for an edge with 0°, 180° and 360° of etched depth under TE (a) and TM (b) polarizations. Normalized amplitude of the near field for an edge with 180° of etched depth and 0nm, 25nm 50nm and 75nm of undercut under TE (c) and TM (d) polarizations. The ideal, sharp edge transition is shown in all cases for comparison. Observe that the "edge response" becomes slower for increasing etched depths and faster for increasing undercuts.

It is instructive to isolate the difference of the true edge scattering from the ideal, sharp edge transition. This is done in Figure 6, which depicts the amplitude of this (complex) difference for all respective plots of Figure 5. Observe that, indeed, by increasing the etched depth the difference has a larger spatial extent, whereas increasing the amount of undercut confines the spatial extent of the difference. This is crucial, because it is exactly the spatial extent of the difference that affects its spectral distribution. If the difference is well confined, its spectral distribution is spread out to higher spatial frequencies and the lower frequency content is small. In such a case the complex difference can be neglected and the approximation of the ideal, sharp transition is adequate. However, when the difference has a larger spatial extent then its lower frequency content becomes significant and it cannot be neglected. This is shown in Figure 7, which depicts the magnitude of the spectra of all respective difference distributions of Figure 6. Observe that the through-the-lens (TTL) spectrum of the difference attains larger values when the etched depth increases and smaller values when the amount of undercut increases, as expected from Figure 5 and Figure 6. The normalization used in spectra plots is that a constant (DC) value of 1 (clear field) would produce a Dirac δ-function at zero frequency with amplitude of 19.4 ($\sqrt{\eta} = \sqrt{\sqrt{\mu_0/\varepsilon_0}} \approx 19.4\Omega$).

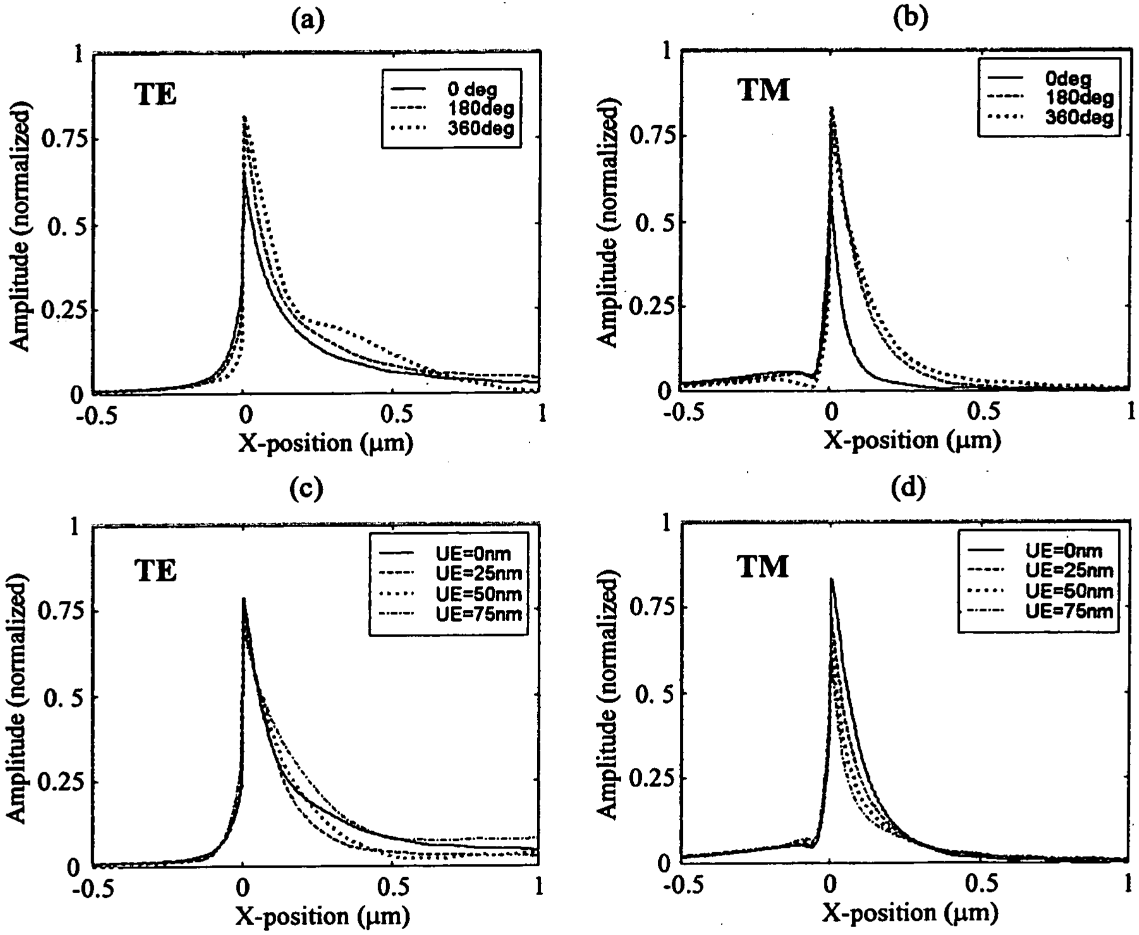

Figure 6. Complex difference of true edge scattering from ideal, sharp transition

The amplitude of the complex difference of the true electromagnetic field scattered from an edge from the ideal, sharp transition (step-function) is shown in (a)-(d) for all edge profiles and illumination polarizations of Figure 5 respectively. (a) and (c) are for TE polarization and (b) and (d) are for TM polarization. The spatial extent of the difference grows with increasing etched depths, as seen in (a) and (b), and shrinks with increasing undercuts, as seen in (d) for TM polarization. The behavior in (c) appears somewhat erratic, but if the phase is also taken into account, it is shown in Figure 7 that this is also the case for TE polarization.

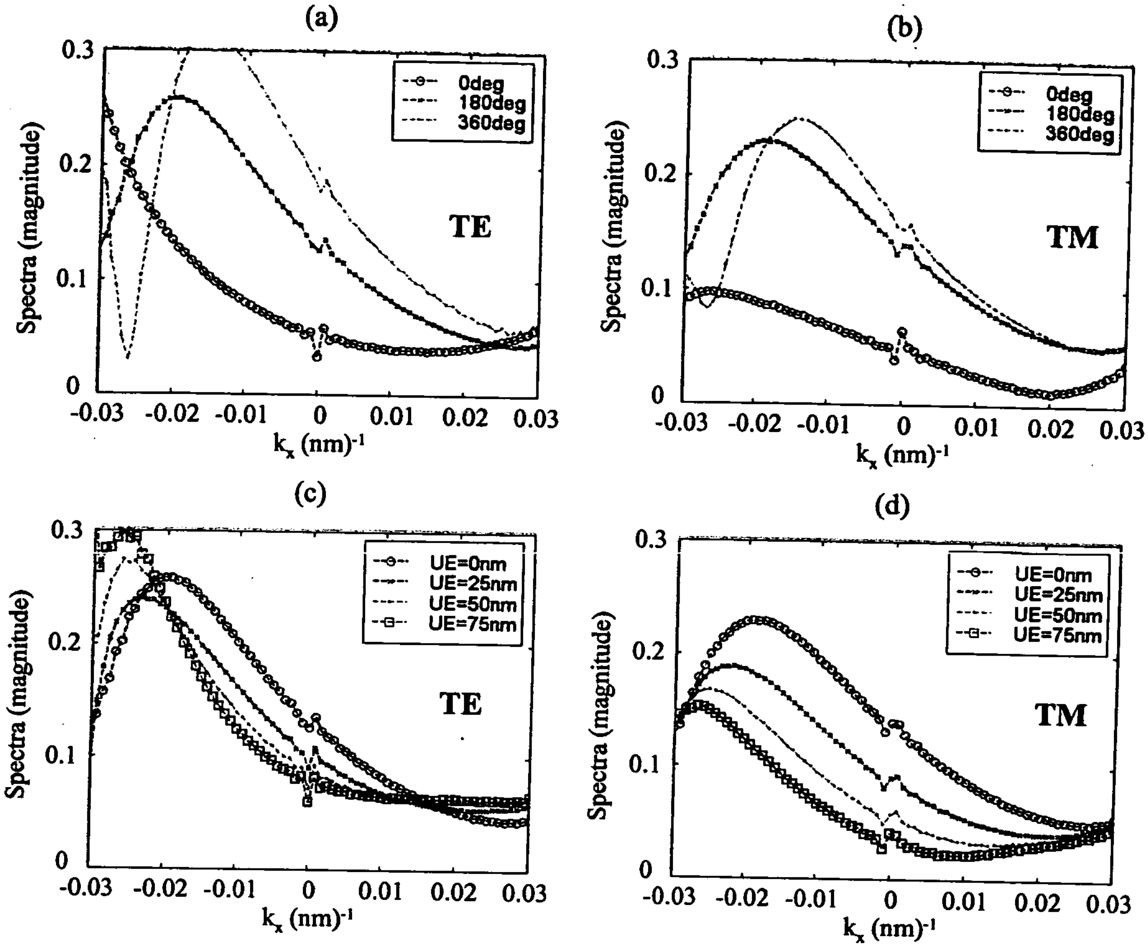

Figure 7. Spectrum of complex difference

The spectra of the complex differences shown in Figure 6 are depicted here respectively. (a) and (c) are for TE polarization and (b) and (d) are for TM polarization. Observe that the through-the-lens (TTL) parts of these spectra, which for typical lithographic imaging situations (R=4, NA~0.7-0.8) extent up to ~ +/- 0.008 (nm)$^{-1}$ are smaller for smaller etched depths and larger undercuts, regardless of polarization, as expected from the observations on the plots of Figure 5 and Figure 6.

3.3. Application of edge-DDM in simple 2D layouts

The application of the edge-DDM on an isolated square hole and an isolated square island (post) and comparison of the results with fully rigorous 3D mask simulations (r-masks) are presented here. The edge profile has a glass etched depth of 180^0 and an undercut of 50nm. The dimensions of both the hole and the island are 400nm x 400nm (4X), corresponding to approximately 2 x 2 wavelengths, for λ=193nm.

Figure 8(a) and (b) depict the amplitude of the scattered field across the observation plane below the hole obtained *via* the edge-DDM and *via* fully rigorous 3D simulation, respectively. The amplitude of their difference (error of the edge-DDM) is shown in Figure 8(c). Locally the amplitude of the error is seen to reach a discouraging level of almost 50% of the clear field value. The normalized mean square error is however more contained and is only about 4.9% if calculated within a 3μm by 3μm area or 3.6% if calculated within the 0.4μm by 0.4μm open area of the hole, as shown in Figure 8. However, neither of these error levels is immediately relevant in the simulation of the image formation. What is rather more relevant is the error incurred on the diffraction orders that are collected by the imaging optics. If the spatial frequencies of the error depicted in Figure 8(c) are sufficiently high, this error will be discarded by the projection lens. This concept is shown in Figure 9, where

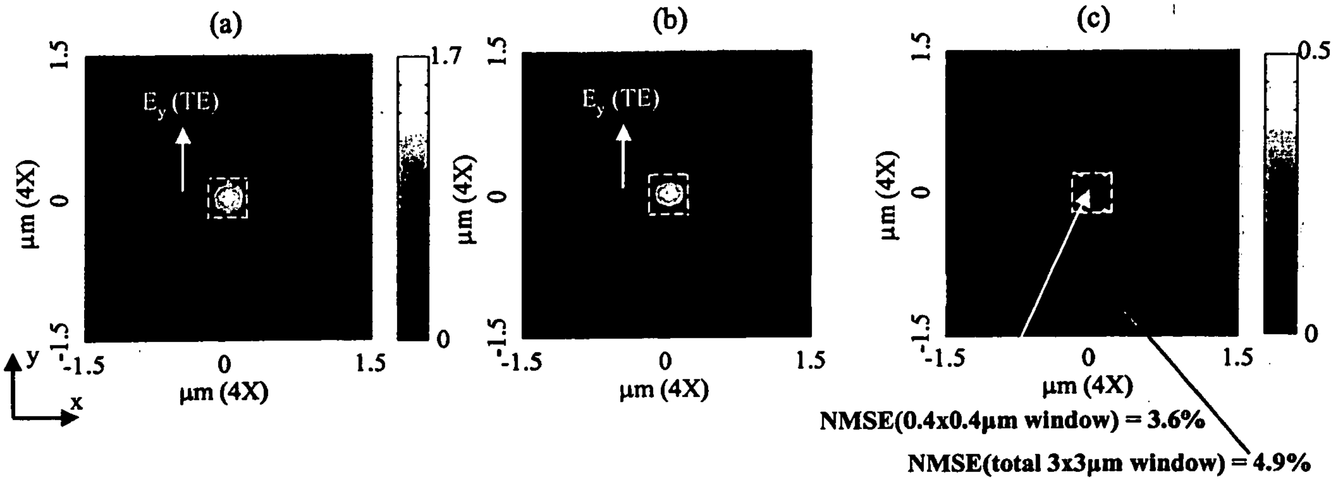

NMSE(0.4x0.4μm window) = 3.6%

NMSE(total 3x3μm window) = 4.9%

Figure 8. Edge-DDM applied on an isolated square hole (scattered field)

(a) Synthesized with the edge-DDM and (b) rigorously calculated scattered field (amplitude), across the observation plane below a 400nm x 400nm isolated hole. A 180° etch and 50nm undercut has been applied. The amplitude of the error (difference of r-mask from edge-DDM) is shown in (c). Locally the amplitude of the error reaches the 50% level, but the normalized mean square error does not exceed 5%.

the spectra (magnitude) of the scattered fields from edge-DDM and from rigorous 3D simulation are shown in (a) and (b) respectively. The marginal circles indicating the propagating plane waves (with $|\vec{k}| \le 2\pi/\lambda$) and the collected by the imaging system plane waves (with $|\vec{k}| \le 2\pi NA(1+\sigma)/\lambda R$), for NA=0.75, R=4 and σ=0.3, are indicated on these plots. The magnitude of the error in the spectrum of the field obtained from edge-DDM is shown in Figure 9(c). Observe that most of the error is concentrated in the higher spatial frequencies for $|k_x|$ approaching 0.03 and only small levels of error exist in the collected orders. The normalized mean square errors of all propagated and collected orders are 2.2% and 2E-4 respectively.

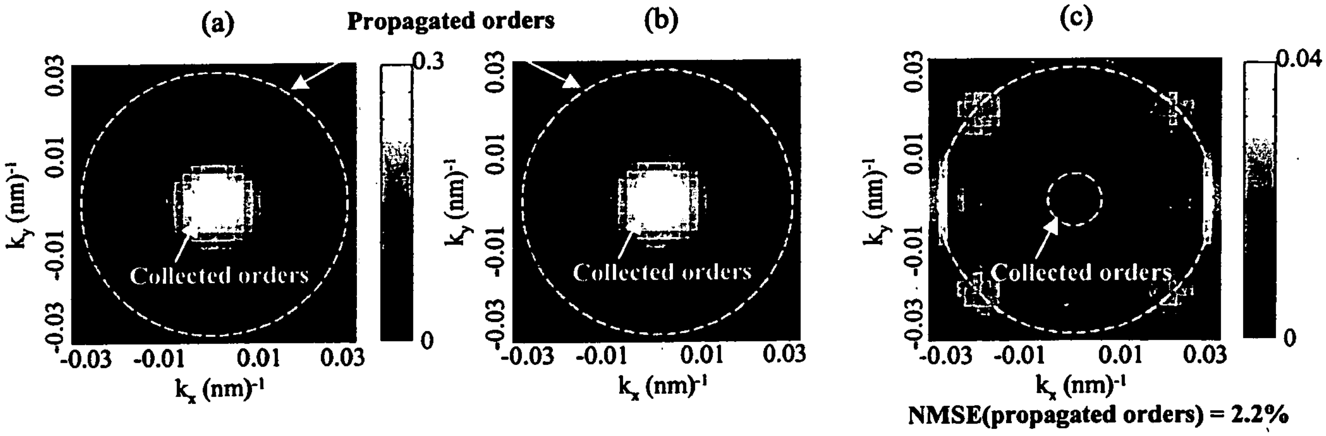

NMSE(propagated orders) = 2.2%

NMSE(collected orders) = 2e-4

Figure 9. Edge-DDM applied on an isolated square hole (spectrum)

Magnitude of the plane wave spectra of the near field plots in Figure 8. Spectrum of the synthesized (edge-DDM) field in (a) and of the rigorous field (from 3D simulation) in (b). The spectrum of the error is depicted in (c). The error level within the collected orders circle is seen to be an insignificant 0.02%.

Similarly, the amplitude of the scattered fields across the observation plane below the isolated island obtained with the edge-DDM and with fully rigorous 3D simulation and the amplitude of the error are shown in Figure 10. Again, a locally significant error amplitude near the corners is evident. However, the energy of this error is concentrated mostly at the higher spatial frequencies, for $|k_x|$ approaching 0.03 and the error in the collected orders is seen to be very small, only 0.16% in a NMSE sense. Note that the large DC component of the isolated island mask layout was subtracted in order to make meaningful comparisons of the edge-DDM with fully rigorous simulations. Otherwise this large DC component would artificially show an even better accuracy, since the error level in comparison with a much stronger signal (containing the DC term) would be smaller.

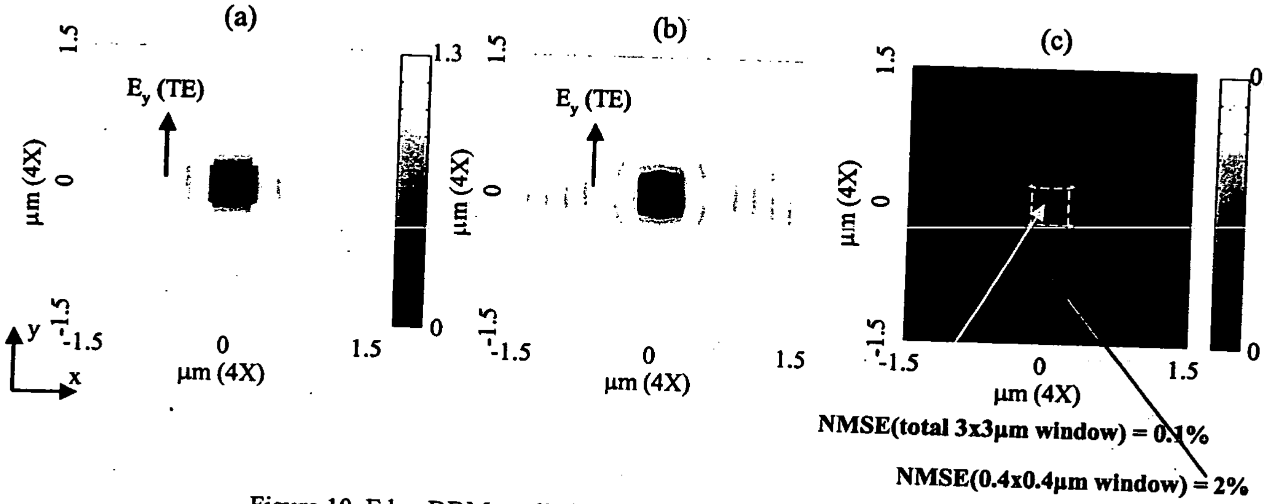

NMSE(total 3x3µm window) = 0.1%

NMSE(0.4x0.4µm window) = 2%

Figure 10. Edge-DDM applied on an isolated square island (scattered field)

(a) Synthesized with the edge-DDM and (b) rigorously calculated scattered field (amplitude), across the observation plane below a 400nm x 400nm isolated island (post). A 180° etch and 50nm undercut has been applied. The amplitude of the error (difference of r-mask from edge-DDM) is shown in (c). Locally the amplitude of the error reaches the 50% level, but the normalized mean square error does not exceed 2%.

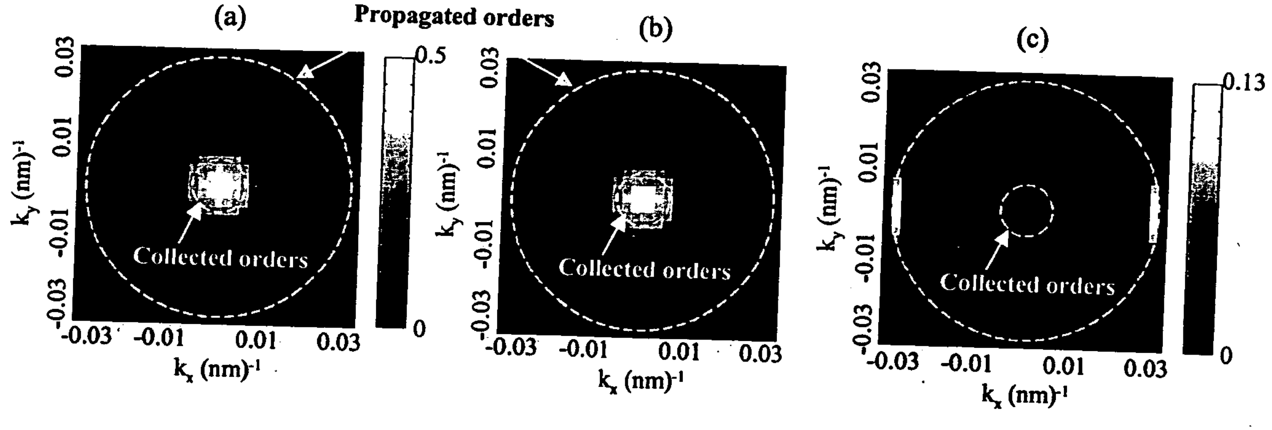

NMSE(propagated orders) = 4%

NMSE(collected orders) = 0.16%

Figure 11. Edge-DDM applied on an isolated square island (spectrum)

Magnitude of the plane wave spectra of the near field plots in Figure 10. Spectrum of the synthesized (edge-DDM) field in (a) and of the rigorous field (from 3D simulation) in (b). The spectrum of the error is depicted in (c). The error level within the collected orders circle is only 0.16%.

It is worth mentioning that each fully rigorous mask simulation that was performed with TEMPEST used approximately 1.8Gbytes of memory and required almost 2 days on a 550Mhz CPU. On the other hand, once all of the required 2D edge simulation results are available the scattered field can be obtained with the edge-DDM in less than 1sec! It should be stressed once again here that the simulation of the isolated edge diffractions is an off-line procedure. It only needs to be performed once and the edge-diffraction results are recycled as many times as are necessary for the reconstruction of the scattered fields of arbitrary layouts. In the above examples, it took approximately 5min for each rigorous, isolated-edge 2D simulation.

3.4. Example of edge-DDM on a large, arbitrary layout of a 0°/90°/270° alt. PSM

The edge-DDM is used here to generate the scattered field from a three level (0°/90°/270°) alt. PSM. A portion of the arbitrary target layout is shown in Figure 12 before and after the phase assignment. The rectangle and edge extraction according to the algorithm presented in Section 3.1 is performed within the 3μm by 4μm (1X) coherence window shown and the scattered field obtained with the edge-DDM inside the 12μm by 16μm (4X) coherence window is also shown in Figure 12 for TE and TM illuminations at λ=193nm. Note that a fully rigorous 3D mask simulation of a 12μm by 16μm (4X) layout would require close to 40Gbytes of memory and would only be feasible on a multi-CPU architecture. The scattered field is obtained with the edge-DDM implementation in less than 1min. This time includes the polygon and edge extraction and the field synthesis from pre-calculated edge diffractions. Therefore, the results of the edge-DDM cannot be immediately compared with a fully rigorous solution, but the accuracy of the edge-DDM within the imaging system's collection ability can reveal the inaccuracies of the ideal k-mask, where all transitions are assumed perfectly sharp. This is done in Figure 13, where the images (at

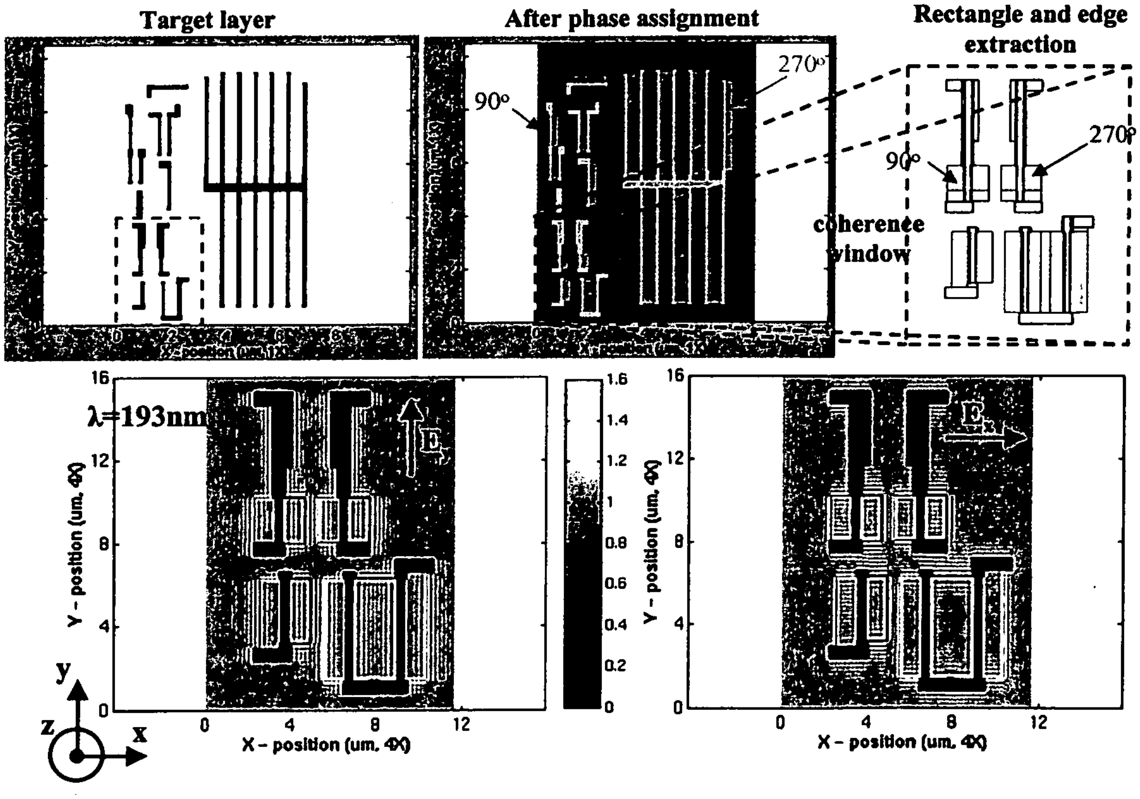

Figure 12. Example: Edge-DDM on a large 2D mask layout (algorithm and near fields)

The target mask layer and the mask after assignment of an arbitrary layout are shown. A three phase-level alt. PSM is assumed (0°/90°/270°). The rectangle and edge extraction within the 3μm by 4μm (1X) coherence window for the various polygons is also shown. Finally, the scattered near field within the coherence window for both TE and TM (λ=193nm) illumination is depicted.

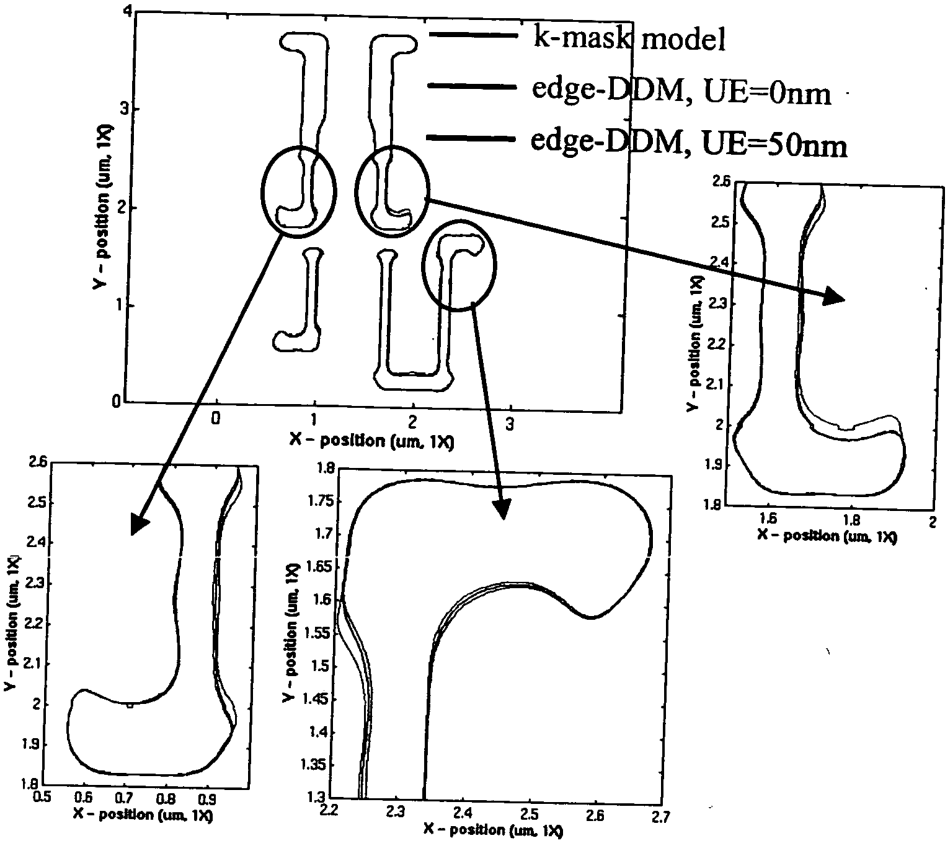

Figure 13. Example: Edge-DDM on a large 2D mask layout (images)

Image (30% intensity contours) of the layout within the 3μm by 4μm (1X) coherence window of Figure 12. The ideal k-mask (Kirchhoff-mask) model is compared with the edge-DDM for an undercut of 0nm and 50nm. The edge-DDM is capable of revealing the inaccuracies of the k-mask model and of accurately taking into account the edge scattering of different edge profiles.

the 30% intensity level) obtained with the k-mask and the edge-DDM for two different undercuts (0nm and 50nm) are compared. The system parameters are λ=193nm, NA=0.7, σ=0.3 and R=4. The inaccuracies of the k-mask model are revealed at various locations in the image as seen in Figure 13. The effect on the image of changing the undercut from 0nm to 50nm can be quickly and accurately evaluated. Observe the subtle differences evident in the intensity contours of the 0nm and 50nm masks of Figure 13.

4. SPEEDING-UP FURTHER THE EDGE-DDM

Although the edge-DDM presented earlier achieves excellent accuracy and tremendous speed-ups as compared to a fully rigorous mask simulation, there is still one more parameter to exploit in order to further speed-up the method. As was shown in [1], where the matched Kirchhoff mask model (mk-mask) was developed, there is no need to carry all the details of the true field scattering as far as the imaging process is concerned (with larger than 1 reduction factors), since the higher spatial frequencies are not used. If a lumped parameter model can be devised that closely matches the through-the-lens (TTL) spectrum of the scattered field then the task of an accurate field representation is accomplished. In [1] a rect-function was seen to very successfully mimic the TTL spectra of scattered fields from various size and profile openings. A similar principle can be applied here with the purpose of matching the TTL spectra of edge-diffracted fields. Assuming a restriction to piecewise constant models, the scattered field from an isolated edge under TE or TM illumination can be approximated using the multi-step functions shown in Figure 14. Although not shown in Figure 14, the amplitude, phase and size of all steps are optimized

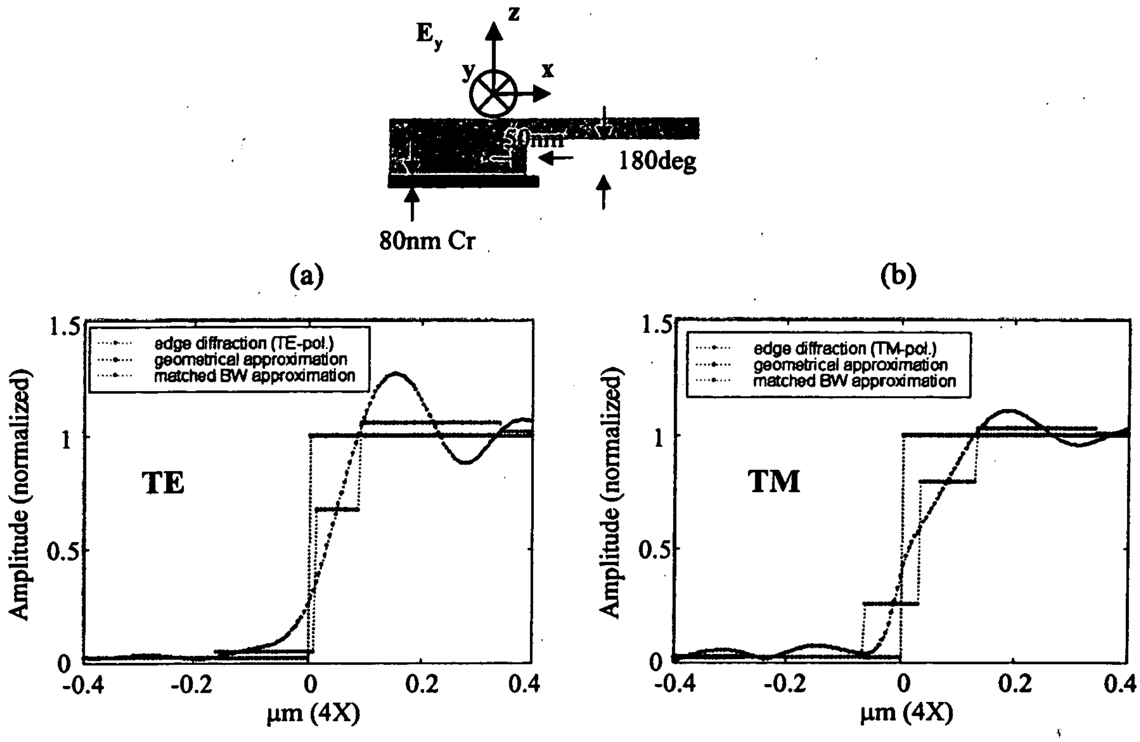

Figure 14. Matched bandwidth approximation to edge diffraction

Instead of approximating the true edge diffraction by a single step function (geometrical or Kirchhoff approximation) a multi-step piecewise constant function is employed. The amplitudes, phases and sizes of all steps are optimized to achieve the best spectral matching of the collected orders with the orders resulting from the continuous edge diffracted field. The matched bandwidth approximations to the field diffracted by a 180° edge with 50nm undercut under TE and TM illuminations are shown in (a) and (b) respectively.

to achieve the best spectral matching of the collected (TTL) orders with the orders resulting from the continuous edge-diffracted field. Note that the key factor for a good spectral match is to capture the finite extent of the "off-on" edge transition. A piecewise constant function is not the best choice to achieve this task, but on the other hand a piecewise constant function offers a good lumped parameter approach and it lends itself nicely as an extension of the unmatched Kirchhoff approach, where all edge transitions are assumed perfectly sharp.

If the matched bandwidth edge-DDM is applied on the 400nm by 400nm (4X) isolated hole of Figure 8 the scattered field across the observation plane can be represented in the compact way shown in Figure 15(a). Recall that the edges parallel to the y-axis "see" TE polarization and the edges parallel to the x-axis TM polarization. The multi-step matched BW approximations to the edge diffraction shown in Figure 14 for TE and TM illuminations intermingle in the x- and y-directions to produce the multi-color mask of Figure 15(a), where each color represents a different amplitude and phase region of the mask. The spectrum of the error of this approach is depicted in Figure 15(b). Note that compared to the error shown in Figure 9(c) this error has increased by almost four-fold. Nevertheless, the error in the TTL spectrum still remains at low enough levels for accurate imaging simulations. A better approximating function, other than the piecewise constant step function, that is more capable of capturing the true edge-diffraction profile (such as linear or higher order polynomial) should result in better spectral matching and consequently more accurate imaging simulations.

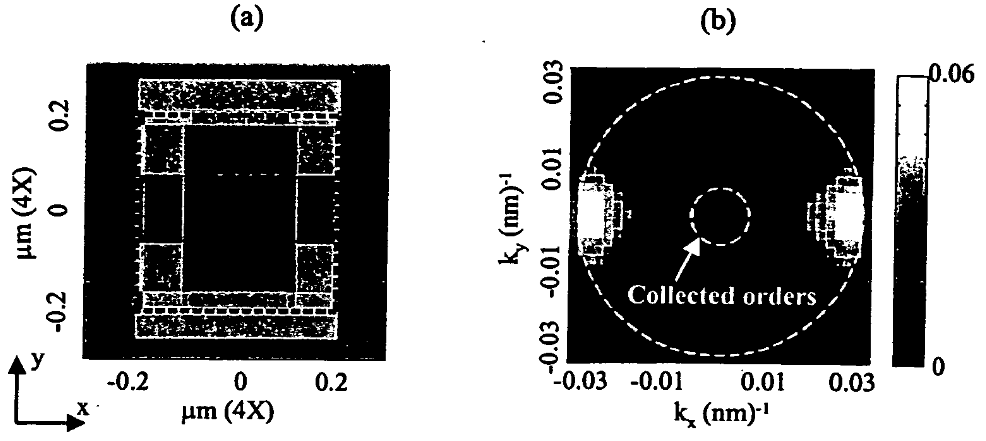

NMSE(propagated orders) = 5.7% (was 2.2%)

NMSE(collected orders) = 8.6e-4 (was 2e-4)

Figure 15. The matched BW edge-DDM applied to the hole of Figure 8

(a) Representation of the scattered field below a 400nm by 400nm hole (etched depth 180°, undercut=50nm) using the matched bandwidth edge-DDM, as shown in Figure 14. Each color represents a different amplitude and phase region of the mask. The spectrum of the error of the representation shown in (a) compared to the true solution of Figure 8(b) is depicted in (b). The error level within the collected orders circle is seen to increase from 0.02% to 0.086%.

5. CONCLUSIONS

This paper has dealt with the development of the edge-DDM (edge domain decomposition method). This method is an extension of the domain decomposition method proposed and developed in [1] that introduces tremendous versatility, since only a small number of isolated edge diffraction simulations is shown to contain all the necessary information for the synthesis of the scattered field from arbitrary 2D mask layouts and subsequent accurate imaging simulations. The limits of this method are reached when the mask features are smaller than a wavelength in size and the vertical mask topography is large. Through a systematic process it was determined that features as small as at least 200nm bearing 270° of phase-wells can be accurately decomposed *via* the edge-DDM, at λ=193nm. The method was tested for simple 2D layouts, where rigorous mask simulations are possible. Excellent accuracy accompanied by speed-up factors of 172,800 (1sec *vs*. 2days) were demonstrated. The accuracy of the method was attributed to the fact that on one hand the edge diffraction phenomena are modeled rigorously through 2D edge-diffraction simulations and that on the other hand the errors incurred during the synthesis (primarily near the corners) are mapped at the extremities of the spectrum of propagating waves and do not contribute to the image formation. It was emphasized that all necessary rigorous 2D simulations of the diffraction from isolated edge-profiles is performed off-line and recycled for the diffraction calculation of arbitrary layouts. If needed, the accuracy of the edge-profile diffraction simulations can be pushed to extreme limits, since it is performed only once. This can aid for example in the correct simulation of unusual edge-profiles whose geometrical details would require excessive discretization of the domain. It was also shown that the exact details of the edge-diffraction are not necessary for accurate imaging simulations (with larger than 1 reduction factors) and a piecewise constant, multi-step edge transition model that matches the through-the-lens (TTL) spectrum was introduced. The range of validity of the edge-DDM is expected to be appropriate for rapid and accurate evaluation of aerial images whenever speed is critical, as for example in full-chip OPC software and data-to-database comparisons in the inspection of alt. PSMs.

method", in which the rect-CMTF, which is now a function of both x, y, is determined independently for the x- and y- directions of the alt. PSM. A total of only four 2D rigorous EM simulations are required (shown in Figure 14(a) as cut-lines 1-4) that take just under 8min to run and utilize negligible memory (~3Mb). Note that in this example the cross-talk can be neglected (the 50nm of underetch virtually eliminated cross-talk between adjacent features) and the mask decomposition follows Figure 3.

The agreement of the "accurate scalar CMTF method" with the full 3D rigorous EM field simulation is spectacular. The image intensity contours at 30% of the clear field virtually overlap and the same is true for the aerial images at the cut-line that runs through the center of the contact holes, as shown in Figure 14(b) and 14(c). For comparison, the aerial image contours and at the same cut-line of the scalar CMTF without adjustment is also shown on these plots.

Three-dimensional simulation results from other dark-field alt. PSM layouts (dense line/space pattern, corners) were also used to benchmark the "accurate scalar CMTF method" with equally successful outcomes. The ~400X speed-up achieved in the example presented would have been approximately halved for a discretization of 25 cells per λ. The speed-up resulting from this method depends on the size of the 2D mask layout, the discretization chosen for the rigorous EM field simulations and the number of rectangles that constitute the layout of the dark-field alt. PSM.

6. CONCLUSIONS

Rigorous electromagnetic simulation of the role of the mask in the imaging process has so far been limited to 2D problems and relatively small periodic 3D problems. Although this capability is enough to tackle a variety of advanced photomask design issues, it is unquestionably very restrictive. For example, rigorous simulation of a 10μm by 10μm area on an alt. PSM that contains random (non-periodic) structures, at λ=193nm, would require on the order of ~3.6Gb of memory (discretization of the ~14,000λ^3 domain with 20 cells per λ) and would run for many hours on a powerful CPU. Although the scalar theory can handle large mask domains, it has been discarded for advanced photomask technology simulations as being inaccurate. In this article, we have demonstrated a way to improve the accuracy of simulations with the scalar theory via the "accurate scalar CMTF method". This method involves using scalar CMTF (complex mask transmission function) models of single openings that are tuned to provide excellent spectral matching with the rigorously calculated CMTF inside a band of interest. A simple scalar CMTF model, namely the rect-CMTF, was presented and the effect of its three parameters on the spectrum was thoroughly investigated. The "accurate scalar CMTF method" is capable of better than 99% agreement with the vector theory and huge computational speed-ups, on the order of 200X or better, can be realized. Model-based CAD tools, that so far rely on scalar theory for aerial image calculations, can be tuned to be very accurate. Conceivably, accuracy in par with a rigorous 3D simulation becomes feasible for large - even full mask - areas.

The way to decompose an alt. PSM into many constituents that properly account for the cross-talk between phase-wells was demonstrated, as an integral part of the "accurate scalar CMTF method". Through this decomposition, a much deeper understanding of the physical phenomena that take place at the corners and at the edges of phase-wells of alt. PSMs arose. Specifically, the corners and edges at the bottom of the phase-wells were identified as the sources of cross-talk between adjacent phase-wells and it was found that the amount of light due to cross-talk becomes significant for alt. PSM technologies deeper than 90°/270°.

ACKNOWLEDGEMENTS

The lithography research was supported by industry and the State of California under the SMART program SM97-01.

REFERENCES

[1] M. Born, E. Wolf, *Principles of Optics*, (Cambridge Univ. Press, 7th ed.), pp. 619-626

[2] US Patents 5,242,770 (Sep. 7, 1993) and 5,447,810 (Sep. 5, 1995) by J.F. Chen and J.A. Matthews

[3] C. Friedrich, L. Mader, A. Erdmann, et. *al.*, "Optimising Edge Topography of Alternating Phase Shift Masks Using Rigorous Mask Modeling", *Proc. SPIE*, Vol. 4000

[4] J. W. Goodman, *Introduction to Fourier Optics*, (McGraw-Hill, 2nd ed.), pp. 55-58

[5] ibid., pp. 33-34

[6] S. Hotta, T. Pistor, K. Adam, A.R. Neureuther, "Effects of Shifter Edge Topography on Through Focus Performance", *Proc. SPIE*, Vol. 4186

[7] J.D. Jackson, *Classical Electrodynamics*, (Wiley, 2nd ed.), pp. 638-641

[8] M.D. Levenson, N.S.Viswanathan, R.A. Simpson, "Improving Resolution in Photolithography with a Phase-Shifting Mask", *IEEE Transactions on Electron Devices* 29(1982), pp.1828-1836

[9] C. Pierrat, A. Wong, S. Vaidya, "Phase-Shifting Mask Topography Effects on Lithographic Image Quality", *IEDM Tech. Digest*, pp. 53-56, 1992

[10] T. Pistor, *Expanding the Simulation Capability of TEMPEST*, Electronic Research Laboratory, University of California, Berkeley, 1997

[11] T. Pistor, A.R. Neureuther, R. Socha, "Modeling Oblique Incidence Effects in Photomasks", *Proc. SPIE*, Vol. 4000

[12] J.R. Sheats, B.W. Smith, *Microlithography - Science and Technology*, (Marcel-Dekker, 1998), ch. 3

[13] K. Toh, *Two-Dimensional Images with Effects of Lens Aberrations in Optical Lithography*, M.S. Thesis, University of California, Berkeley, 1988

[14] Wong, A., *Rigorous Three-Dimensional Time-Domain Finite Difference Electromagnetic Simulation*, Electronics Research Laboratory, University of California, Berkeley, 1994

[15] A. Wong, A.R. Neureuther, "Mask Topography Effects in Projection Printing of Phase Shift Masks", *IEEE Transactions on Electron Devices* 41(1994), pp. 895-902

[16] www.millennium.berkeley.edu